15th Australasian Wind Engineering Society (AWES) Workshop
Sydney, Australia
23-24 February, 2012

The effect of turbulence on near wake structure of a horizontal axis wind turbine wake

M. Sherry [1], J. Sheridan [1] and D. Lo Jacono [1,2,3]

[1]Fluids Laboratory for Aerospace and Industrial Engineering, Department of Mechanical and Aerospace Engineering, Monash University, Victoria, 3800, Australia

[2]Université de Toulouse; INPT, UPS; IMFT; Allée Camille Soula, F-31400 Toulouse, France.

[3] CNRS; IMFT; F-31400 Toulouse, France

Abstract

The instability mechanisms affecting the vortical wake of a specially designed model horizontal axis wind turbine are investigated using particle image velocimetry in a water channel facility. The wake of the tower structure causes a faster degeneration of the tip vortices in the lower half of the wake compared to those in the upper half of the wake. It is found the tip vortices in the upper half of the wake become unstable due to the mutual induction between adjacent tip vortices. Freestream turbulence intensity is seen to adversely affect the tip and root vortex formation such that the coherent structures cease much closer to the rotor plane compared to a low turbulence inflow case. Both the tip and root vortices are captured allowing detailed analysis of the evolution of these helical vortices.

Introduction

The near wake of a horizontal axis wind turbine (HAWT) contains N tip and root helical vortices shed from each of the N blades. Turbines in wind farms may be subjected to these coherent structures if the cluster density is too large. These vortical structures are important from a wind farm planning viewpoint as they can induce increased fatigue loading which is difficult to predict.

It is thus important to investigate the vortical structures in the near wake of a HAWT to determine their interaction and evolution. Field measurement campaigns whilst desired, are difficult from both a logistical and financial viewpoint. Small scale studies are thus undertaken in controlled conditions to investigate the helical vortices in a wind turbine wake. Small scale studies however suffer from Reynolds number effects with a reduction in airfoil perfomance the primary concern. Geometric scaling of full scale turbine geometries is unsuitable for vortex dynamics investigations due to the poor performance of the airfoil section at the scaled Reynolds number. A clean vorticity signal is paramount in helical vortex dynamics investigations to ensure interaction and evolution of the coherent structures can be attributed to instability mechanisms. Detailed blade design is thus required to ensure attached flow and uniform blade loading, $(c(r)C_l(r))$, where $c(r)$ and $C_l(r)$ are the local chord and sectional lift coefficient respectively along the span of the blade.

The tip vortices within HAWT wakes have been investigated using PIV in a uniform (Whale et al, 1996; Dobrev et al, 2008; Grant and Parkin, 2000) and boundary layer (Hu et al, 2011) inflow. These studies provided valuable insight into tip vortex structure (Dobrev et al, 2008; Grant and Parkin, 2000) but all were unable to capture the root vortex due to the model turbine design. The effect of turbulence on the vortical structures in the near wake has not been previously investigated experimentally. Troldborg et al (2007) simulated a HAWT operating in a turbulent inflow numerically with the actuator line technique and noted the wake broke down closer to the rotor plane compared to the uniform inflow case.

This contribution presents near wake data of a specially designed HAWT model for low Reynolds number investigations subjected to elevated freestream turbulence levels. Of principal interest is the instability mechanisms affecting the HAWT wake and the role turbulence plays in this process. The near wake is investigated until the vortices within the wake become unstable.

Experimental apparatus and method

The investigation was conducted in a free surface water channel with dimensions of $4000\times600\times800$ mm. The free stream speed is adjustable in a range of 60mm/s to 460mm/s. An optimum Glauert rotor was specifically designed for the low Reynolds number water channel investigations presented here. The blades were optimised using the blade element momentum (BEM) method with heavy rotor and tip correction formulae of Shen et al (2005) applied. The design tip speed ratio, λ_d, which is the ratio between the tip speed and the free stream velocity, as defined in equation 1 was 3.5.

$$\lambda = \frac{\Omega R}{U_\infty} \tag{1}$$

where Ω is the rotational speed of the turbine blades, R is the rotor radius and U_∞ is the freestream velocity.

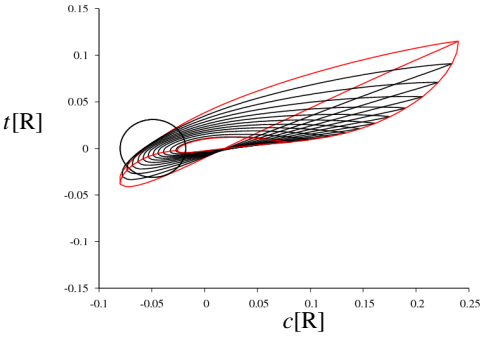

Figure 1: Glauert rotor twist and chord variation illustrating the highly twisted nature of the blade to maintain the prescribed angle of attack. Origin is at the quarter chord position. Tip, root chord and leading and trailing edges of blade shown in red for clarity.

The rotor blades have a radius of $R = 115$ mm, and contain both twist and taper to minimise spanwise variations in blade loading $(c(r)C_L(r))$, where $c(r)$ and $C_L(r)$ are the local blade chord and sectional lift coefficient respectively. A uniformly loaded blade is crucial for HAWT vortex stability studies to minimise the variation in the vorticity sheet emanating from the blade trailing edge. The lifting surface purposely terminates outside the influence of the nacelle boundary layer to minimise effects of turbine support geometries on root vortex formation. A linear blending function was used between the root region lifting

surface termination point ($0.245R$), and the cylindrical section which connects to the hub. The twist and chord distribution of the final design is shown in figure 1.

A stepper motor with micro-stepping drive (OEM350-650, Parker) and controller (6K2 controller, Parker) provided the torque to drive the turbine and achieve truly controlled experimental conditions. With proper analysis of the forces acting on the turbine, the near wake of a HAWT is equivalent between driven and freely spinning model turbines. The upper drive shaft situated above the water channel was synchronised to the turbine main shaft by a timing belt that passed through the turbine tower support geometry. An optical encoder (HBM5–1250, US Digital) attached directly to the upper drive shaft and synchronised the data acquisition sequence to a specified blade azimuthal position. In the measurements, a blade was aligned with the tower section and hence in the image plane.

A CCD Particle Image Velocimetry (PIV) camera with a resolution of $4\,008 \times 2\,672$ pixels was used in conjunction with a 105 mm lens to acquire the velocity fields. A multi-step interrogation window with final size of 32×32 pixels with 50% overlap was used. This allowed instantaneous velocity maps of 249 by 166 vectors to be captured. A total of 600 independent image pairs were captured for each turbine position and turbulence setting with convergence occurring prior to 400 image pairs. Validated cross correlation PIV software developed in-house was employed to generate the displacement fields (Fouras et al, 2008).

Turbulence grids

The freestream velocity can be decomposed into mean and fluctuating velocity components as $U = \overline{U} + u$. Turbulence intensity is characterised by the root mean square (*rms*) of the fluctuating velocity component as shown in equation 2.

$$I_u = u_{rms}/U_\infty \tag{2}$$

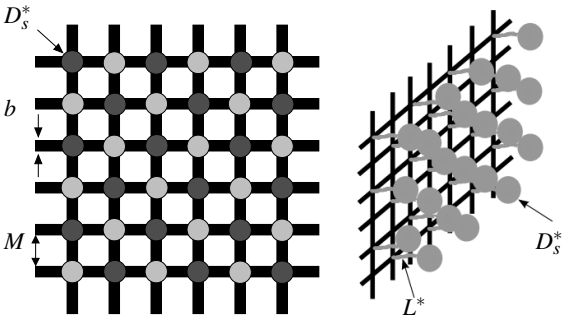

Figure 2: Novel tethered grid design from Vonlanthen and Monkewitz (2011). Left: Tethered sphere turbulence grid with mesh size, M, bar size, b, and sphere diameter to mesh size ratio, $D_s^* = 0.75$. Shade of sphere indicates tether length, light: $L^* = 1.5$, dark: $L^* = 2$. Right: isometric view of tethered sphere grid, only spheres of a single tether length are shown for clarity.

To elevate the freestream turbulence intensity, a novel 'tethered sphere' turbulence grid (TSG) design was constructed (Vonlanthen and Monkewitz, 2011). The TSG used a grid with mesh size, $M = 50.8$ mm and bar size, $b = 6$ mm as the base structure. Tethered spheres were attached to the grid nodes as shown in figure 2 to improve mixing and isotropy of the turbulence generated. The spheres were constructed of celluloid ('table tennis') balls of diameter 38 mm, which were filled with water to minimise buoyancy effects. The current TSG design operated with a sphere diameter to mesh size ratio, $D_s^* = D_s/M \sim 0.76$, shown to produce the largest turbulence intensity (Vonlanthen and Monkewitz, 2011). The tether lengths, $L^* = L/D_s$, varied from $1.5 - 2$ to ensure freedom of movement arising from vortex induced vibration of the tethered spheres. An isometric schematic of the TSG is shown on the right in figure 2. The TSG was positioned at $x/M = 28$ or $12.5R$ from rotor plane. The turbulence intensity of the TSG was evaluated using a 2D laser doppler velocimetry (LDV) system and a 3-axis traverse (IMC-S8 controller, ISEL). The turbulence intensity at the rotor location was 6.2%.

Results

In the following section, phase locked vorticity maps of the helical vortex wake behind the model HAWT will be presented. The phase locked vorticity map of the near wake of the HAWT operating close to the design tip speed ratio of λ_d is shown in figure 3.

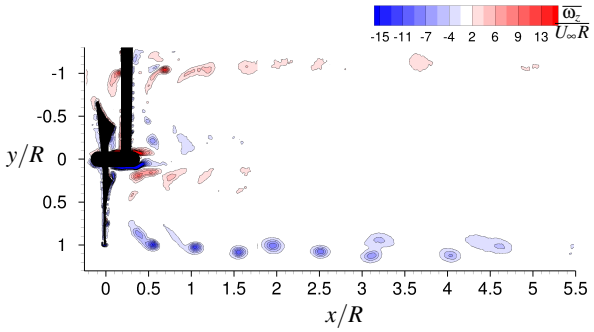

Figure 3: Near wake vorticity contour plot near the design tip speed ratio, $\lambda = 3.55$. Tip vortices are seen in both the upper (blue) and lower (red) halves of the wake. Root vortices are also seen in the upper (red) and lower (blue) halves of the wake. The vortices in the lower half of the wake are 60° younger than those in the upper half of the wake. The vortices in the lower half of the wake degenerate at a faster rate than those in the upper half due to the wake of the tower structure.

The dominant near wake vortical structures, the tip and root vortices are clearly evident. Coherent tip vortices are present at $y/R \approx \pm 1$ and root vortices at $y/R \approx \pm 0.2$ in the top ($y \geq 0$) and bottom ($y \leq 0$) halves of the wake. The orientation of the vortices in the two halves is opposite due to the different orientation of the helical filaments. The tip vortices in the lower half of the wake are 60° younger than those in the upper part of the wake due to the phase locking technique.

In the three filament system shown in figure 3, mutual induction between adjacent tip vortices leading to instability and filament entanglement initially occurs between two filaments. Felli et al (2011) noted that the initial entanglement of the helical tip vortices behind a marine propeller was dependent on the number of blades. For a three-bladed propeller, tip vortex entanglement initially occurs between two filaments while the remaining filament is little affected. The same phenomena was also evident in the early visualisations of Alfredsson and Dahlberg (1979) but is shown here for the first time with quantitative data in a HAWT wake.

The first indication of mutual inductance between adjacent tip vortices in the upper half of the wake becomes evident in figure 3 for $x/R \geq 1.5$. The interacting tip vortices are 360° and 480° old respectively, where vortex age (VA) is defined as the azimuthal travel of the blade since filament creation in degrees (°). The younger vortex ($VA = 360°$) moves radially outward

relative to the older vortex ($VA = 480°$) due to the mutual induction between the two tip vortices. As the two interacting tip vortices advect further into the wake, entanglement and interaction progresses, as evident at $x/R \sim 3.15$, where the vortices are now 720° and 960° old. By $x/R \sim 4.5$, vortex coalescence has occurred fully and the two tip vortices appear as a single patch of vorticity. The signal of the coalesced tip vortices decreases rapidly thereafter due to the spatial smoothing of the phase locking technique. The same phenomena is difficult to discern in the bottom half of the wake due to the faster degeneration of the tip vortices.

An important finding confirmed by figure 3 is the detrimental affect the tower has on the vortices within the wake. With the current model setup, the tower section commences at $x/R = 0.18$. Based on the pitch of the helical filaments, which is the axial distance a tip vortex travels in a complete revolution, the tip vortices in the lower half of the wake will interact with the tower section at 60°. The first tip vortex in the lower half of the wake is thus interacting with the tower support structure in figure 3. The turbine tower is elliptical in shape and will create a vortex system similar to a von-Karman vortex street in isolation. The axis of the von-Karman vortices are perpendicular to the freestream velocity and hence they are not seen in the current planar measurements. It is evident from figure 3 that the turbine tower affects the stability/rate of degeneration of the tip and root vortices in the lower half of the wake. We show for the first time the tip and root vortices in the lower wake half degenerate at a faster rate than those in the upper wake half due to the influence of the tower structure. It is for this reason that phase-locked wind turbine wake studies almost exclusively concentrate on the helical vortex filaments in the upper half of the wake (Grant and Parkin, 2000; Dobrev et al, 2008; Hu et al, 2011).

As the helical vortex filaments in the lower half of the wake are adversely affected by the tower section, only the upper half of the wake is investigated in the elevated freestream turbulence case. The phase averaged vorticity map of model wind turbine subjected to the TSG freestream turbulence operating at a tip speed ratio of $\lambda = 3.73$, is shown in figure 4. The higher tip speed ratio for the TSG case will reduce the pitch of the helical tip vortices emphasising their mutual induction. This effect will be secondary to the increased turbulence intensity.

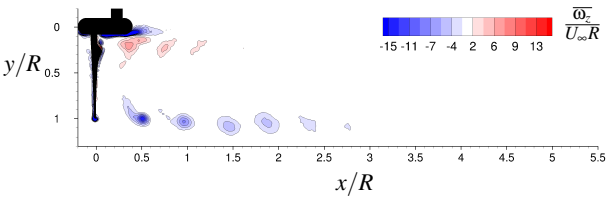

Figure 4: Phase-locked vorticity map of the turbine with high freestream turbulence intensity generated by the TSG close to the design tip speed ratio, $\lambda = 3.73$.

There is an obvious effect of turbulence intensity when figures 3 and 4 are compared. The coherent tip vortices cease much closer to the rotor plane compared to the uniform inflow case. There are three possible reasons for the change in wake topology due to freestream turbulence intensity, they are; increased turbulent diffusion, reduced aerodynamic performance of the rotating airfoil and unsteadiness of the tip vortex formation process leading to increased spatial-smoothing due to phase locked experimental technique. The helical vortices subjected to elevated freestream turbulence intensity have not been investigated experimentally in the past. Each possible mechanism affecting the wake will be discussed below.

Turbulent diffusion:
The turbulent nature of the wake and in particular the Reynolds stresses will enhance diffusion of the vorticity within the wake.

Reduced aerodynamic performance:
It has been shown at higher Reynolds numbers that turbulence effects become appreciable in the stall region around 12° (Swalwell et al, 2004; Sicot et al, 2006). The current blade design is designed to operate with a prescribed 6° angle of attack along the entire span of the blade so turbulence effects will be minimal on the aerodynamic performance of the rotating blades. Further, the local turbulence intensity, $I_{u,r}$, at a blade radial section is less than the freestream value due to the relative velocity which includes blade rotation effects. *i.e* $I_{u,r} = u_{rms}/U_{rel}(r)$, where $U_{rel}(r) = \sqrt{(\lambda(r)U_\infty)^2 + U_\infty^2}$. The local turbulence intensity thus reduces with radial distance from the blade root and is minimal in the region where the majority of torque is generated by the turbine (Sicot et al, 2006).

Unsteadiness of tip vortex formation:
With a turbulent inflow, tip vortex formation will vary each rotation cycle due to the passage of eddies over the blade airfoil. The integral length scale of the generated turbulence is (assumed to be approximately equal to D_s) similar in magnitude to the root chord length. Passage of turbulent eddies over the airfoil will thus alter the uniformity of the trailing edge vorticity sheet which forms into the coherent tip and root vortices. The non-uniformity will lead to increased spatial smooting from the phase-locked measurment technique.

From the above discussion on the effects of turbulence on the near wake vortex structures, turbulent diffusion and the spatial smoothing of the phase-locked measurement technique are the primary mechanisms leading to the differences between figures 3 and 4.

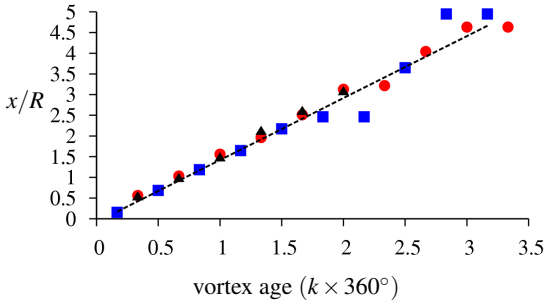

Figure 5: Tip vortex axial position variation with vortex age in the upper and lower wake halves. Low turbulence intensity - red circles: upper wake half tip vortex, blue squares: lower wake half tip vortex. High turbulence intensity - black triangles: upper half tip vortex.

The trajectory of the tip vortices in the upper and lower halves of the wake are shown in figures 5. The freestream turbulence level appears to have little affect on the position of the tip and root vortices as their paths collapse onto a single trend line. A coherent vortex signal persists further in the wake with uniform inflow. The positional trend line is created using the first five vortex realisations and expolated over the entire vortex age domain to highlight deviation from the initial trajectory possibly due to instability mechanisms. Where vortex pairing has occurred in the phase-locked data, the coalesced vortex occupies two vortex age locations. In the uniform inflow results, the interacting vortices in the top half of the wake ($VA = 720°$ and $VA = 840°$) deviate most from the positional trend lines. The third vortex filament, ($VA = 600°$ and later $VA = 960°$) main-

tains its initial trajectory in agreement with the visualisations of Felli et al (2011).

The variation of the maximum value of the squared swirling strength, Λ_{ci}^2 (Zhou et al, 1999) with vortex age is shown in figure 6. Λ_{ci}^2 was used to elucidate the presence of coherent vortical structures as it provides a measure of the local eddying motion within the vortex and discerns rotation from shear. The effect of the tower is obvious with a rapid reduction in maximum swirling strength. The data suggest the vortices in the bottom half of the wake are less coherent than those in the top half of the wake. This is not unsurprising as the vortices in the tower wake will cause complex vortex filament interactions which when averaged will result in a weaker vortex. The filament reactions are obviously absent in the top half of the wake with the result that the maximum swirling strength varies almost linearly with vortex age. A rapid reduction in the turbulent inflow results is also evident from figure 6. The turbulent tip vortex at a vortex age of $VA = 120^\circ$ is of similar magnitude to the uniform inflow case suggesting minimal turbulence effect on the initial vortex strength. The rapid reduction thereafter can thus be attributed to added turbulent diffusion.

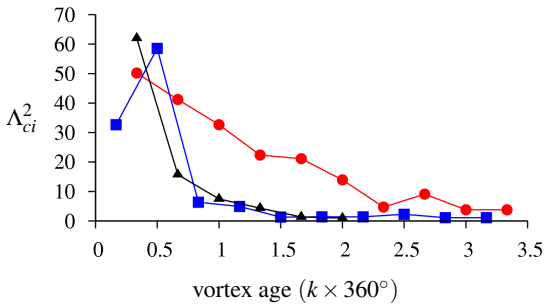

Figure 6: Tip vortex squared swirling strength, Λ_{ci}^2, variation with vortex age in the upper and lower wake halves. Low turbulence intensity - red circles: upper wake half tip vortex, blue squares: lower wake half tip vortex. High turbulence intensity - black triangles: upper half tip vortex.

Conclusion

The near wake of a model HAWT with two levels of freestream turbulence intensity has been investigated with phase locked PIV measurements in a water channel. The tower structure destabilized the wake in the lower wake half at a faster rate compared to the upper wake half. The helical filaments in the upper half of the wake were investigated to determine the instability mechanisms affecting the helical vortex filaments in a HAWT wake. The root vortices diffused closer to the rotor plane compared to the tip vortices. The present data highlighted a mutual inductance mode in the tip vortices with vortex coalescence occurring between two adjacent tip vortices by $4.5R$ downstream. The high freestream turbulence case indicate minimal reduction in turbine performance. The tip and root vortices were weaker in the turbulent inflow case with turbulent diffusion seeing cessation of the vorticity signals closer to the rotor plane compared to the uniform inflow case. The tip vortices in the turbulent inflow case ceased prior to the onset of instabilities. The current data highlight the delicate balance required between helical vortex generation and investigation of turbulence effects.

*

References

Alfredsson P, Dahlberg J (1979) A preliminary wind tunnel study of windmill wake dispersion in various flow conditions. Tech. rep., The Aeronautical Research Institute of Sweden, aU-1499, part 7

Dobrev I, Maalouf B, Troldborg N, Massouh F (2008) Investigation of the wind turbine vortex structure. 14th Int Symp on Applications of Laser Techniques to Fluid Mechanics, Lisbon, Portugal, 07-10 July, 2008

Felli M, Camussi R, Di Felice F (2011) Mechanisms of evolution of the propeller wake in the transition and far fields. Journal of fluid mechanics 682:5–53

Fouras A, Lo Jacono D, Hourigan K (2008) Target free stereo piv: a novel technique with inherent error estimation and improved accuracy. Experiments in Fluids 44:317–329

Grant I, Parkin P (2000) A dpiv study of the trailing vortex elements from the blades of a horizontal axis wind turbine in yaw. Experiments in fluids 28:368–376

Hu H, Yang Z, Sarkar P (2011) Dynamic wind loads and wake characteristics of a wind turbine model in an atmospheric boundary layer. Experiments in fluids (DOI 10.1007/s00348-011-1253-5)

Shen W, Mikkelsen R, Sørensen J (2005) Tip loss corrections for wind turbine computations. Wind Energy 8:457–475

Sicot C, Devinant P, Laverne T, Loyer S, Hureau J (2006) Experimental study of the effect of turbulence on horizontal axis wind turbine aerodynamics. Wind energy 9:361–370

Swalwell K, Sheridan J, Melbourne W (2004) The effect of turbulence intensity on performance of a naca4421 airfoil section. Proceedings of the 42nd AIAA Aerospace Sciences Meeting and Exhibit, 5-8 January, Reno, Nevada (AIAA 2004-665)

Troldborg N, Sørensen J, Mikkelsen R (2007) Actuator line simulation of wake of wind turbine operating in turbulent inflow. Journal of Physics: Conference Series 75:012,063

Vonlanthen R, Monkewitz P (2011) A novel tethered-sphere add-on to enhance grid turbulence. Experiments in fluids 51:579–585

Whale J, Helmis C, Papadopolous K, Anderson C, Skyner D (1996) A study of the near wake structure of a wind turbine comparing measurements from laboratory and full scale measurements. Solar Energy 56(6):621–633

Zhou J, Adrian R, Balachandar S, Kendall T (1999) Mechanisms for generating coherent packets of hairpin vortices in channel flow. Journal of Fluid Mechanics 387:353–396